IEEE Access
Multidisciplinary | Rapid Review | Open Access Journal

Received April 17, 2020, accepted May 9, 2020, date of publication May 14, 2020, date of current version June 3, 2020.

Digital Object Identifier 10.1109/ACCESS.2020.2994620

A Generalized Anti-Interference Low-Ambiguity Dual-Frequency Multiplexing Modulation Based on the Frequency-Hopping Technique

JIANGANG MA AND YIKANG YANG
School of Electronics and Information Engineering, Xi'an Jiaotong University, Xi'an 710049, China
Corresponding author: Yikang Yang (yangyk74@mail.xjtu.edu.cn)

This work was supported by the National Key Research and Development Program of China under Grant 2016YFB0501301 and Grant 2017YFC1500904.

ABSTRACT To improve the anti-interference performance and mitigate the autocorrelation function (ACF) ambiguity of dual-frequency multiplexing modulation, we propose a new type of modulation: frequency-hopping alternated binary offset carrier (FH-AltBOC) modulation based on the frequency-hopping technique. The new modulation is generalized and includes AltBOC modulation, so it inherits the advantages of AltBOC modulation while also exhibiting new properties, such as low ambiguity, low probability of intercept, and better anti-narrowband interference and multipath performance. We first establish the mathematical model, derive the autocorrelation function (ACF) and the power spectrum density (PSD) for the FH-AltBOC modulation. Next, we propose optimal parameters and present a generation and detection scheme. The acquisition time and acquisition complexity of the receiving process for the proposed FH-AltBOC signal are the same as those of the AltBOC signal with the same main-lobe bandwidth (MLB). Finally, we evaluate the performance of several representative FH-AltBOC and AltBOC signals. The results show that FH-AltBOC(24:1:1,1) has the lowest ACF ambiguity, the best anti-interception, anti-narrowband interference, and multipath performance among the considered signals. FH-AltBOC(24:1:6,1) realizes higher tracking accuracy, lower ACF ambiguity, and better anti-narrowband interference and multipath performance than AltBOC(15,10). FH-AltBOC can serve as a new signal design paradigm for global navigation satellite systems (GNSS) and GNSS-like systems.

INDEX TERMS Anti-interference, low-ambiguity, frequency-hopping alternated binary offset carrier (FH-AltBOC), satellite navigation.

I. INTRODUCTION

As demand escalates for large-scale and multitype location-based services, it is becoming necessary to improve the positioning accuracy and the resistance against external interference of global navigation satellite systems (GNSS) and GNSS-like systems in challenging environments such as urban canyons, forested terrains, and indoor areas, in which signal attenuation, interference, and multipath fading severely degrade the positioning accuracy [1], [2]. Meanwhile, navigation applications require GNSS to transmit multiple signals to provide various levels of service, these signals must be combined into a constant-envelope composite signal to maximize high power amplifier (HPA) efficiency and to conserve resources on satellite [3].

Multifrequency multiplexing techniques can combine signals from separate sidebands into a composite signal. Alternated binary offset carrier (AltBOC), which was adopted for the Galileo E5 signal, is dual-frequency constant-envelope multiplexing (DCEM) technique, which combines up to four signal components from two sidebands into a constant-envelope signal by employing multilevel subcarriers [4]. Time-multiplexed offset carrier QPSK (TMOC-QPSK) was proposed to reduce the complexity of signal generation of AltBOC, which uses a BOC subcarrier with time-division multiplexing to combine multiple signal components into a constant-envelope signal [5]. To meet the demands of the BeiDou Navigation System (BDS) signal design, researchers

The associate editor coordinating the review of this manuscript and approving it for publication was Yufeng Wang.

have proposed time-division AltBOC (TD-AltBOC) [6], unbalanced AltBOC [7], generalized AltBOC [8], asymmetric constant-envelope binary offset carrier (ACE-BOC) [9], generalized constant-envelope BOC (GCE-BOC) [10], Interlacing General AltBOC (IGAltBOC) [11], and asymmetric AltBOC [12], which have significant improvements in the flexibility in terms of signal design. Moreover, ACE-BOC with equal length subcarrier segments (ES-ACEBOC) [13] and ACE-BOC with bipolar subcarrier (BS-ACEBOC) [14] were proposed to reduce the implementation complexity of the ACE-BOC. These studies on dual-frequency multiplexing modulation have substantially improved the flexibility of signal design and reduced the complexity of signal generation.

AltBOC modulation can combine up to four signal components and realize outstanding code tracking accuracy and anti-interference performance. However, for higher-order AltBOC modulation, the main drawback is the ambiguity in the code tracking due to the multiple side peaks of the autocorrelation function (ACF) [15]. The receiver may incorrectly lock onto one of these side peaks, causing intolerable measurement bias, this undesirable behavior limits the application of this modulation scheme in navigation systems. In contrast to previous studies, the objective of this work is to define a generalized AltBOC-like modulation that can mitigate the ACF ambiguity and improve the anti-interference performance.

We present a generalized anti-interference low-ambiguity dual-frequency multiplexing modulation based on the frequency-hopping technique, called frequency-hopping alternated binary offset carrier (FH-AltBOC). The proposed FH-AltBOC modulation combines the direct-sequence spread spectrum (DSSS) and the frequency-hopping spread spectrum (FHSS) techniques, which are the most practical and dominant spread spectrum techniques. The basic mechanism of interference suppression in an FHSS system is avoidance: it avoids interference via periodic changing of the carrier frequency of a transmitted signal. The FHSS technique has been widely used in mobile, radar, and military communication systems due to its many advantages, such as the low probability of interception and its resistance to narrowband and multipath interferences [16]–[19]. The generalized FH-AltBOC modulation can be obtained by replacing the subcarrier of AltBOC modulation with frequency-hopping subcarrier, thus, it has the advantages of both the DSSS and FHSS techniques. Since FH-AltBOC modulation implements frequency hopping on the subcarrier rather than on the carrier, it does not affect the performance of carrier-phase measurement and Doppler measurement. The frequency-hopping subcarrier symbols inherit the AltBOC subcarrier symbols to achieve a constant envelope and maintain the flexibility in signal design and implementation.

The remaining sections are organized as follows. First, we formulate the mathematical models of nonconstant-envelope and constant-envelope FH-AltBOC modulations and derive analytical expressions for their ACF and power spectrum density (PSD). We analyze the time and frequency properties of a set of FH-AltBOC signals. Next, we present recommended parameter selections and a generation and detection scheme for the FH-AltBOC modulation. We analyze the characteristics of the ACF and PSD, the false locking probability, the code tracking performance, and the anti-narrowband interference and multipath performance of several specific FH-AltBOC and AltBOC signals. Finally, we present the conclusions. In the appendix, we present the detailed derivation of the analytical ACF expressions for the nonconstant-envelope and the constant-envelope FH-AltBOC modulations.

II. MATHEMATICAL MODEL

Under the assumption that an FH-AltBOC signal has ideal spreading codes and infinite bandwidth, we construct the mathematical models of the nonconstant-envelope and the constant-envelope FH-AltBOC signals and derive their ACF and PSD expressions.

A. NONCONSTANT-ENVELOPE FH-AltBOC

The nonconstant-envelope FH-AltBOC baseband signal can be constructed as the follows:

$$s(t)=\sum_{k=-\infty}^{+\infty}\left[c_{LI}(k)+jc_{LQ}(k)\right]\chi^{*}(t-kT_c,f_s^k)+\left[c_{UI}(k)+jc_{UQ}(k)\right]\chi(t-kT_c,f_s^k) \quad (1)$$

where $c_{LI}(k)$ and $c_{LQ}(k)$, which denote pseudorandom noise (PRN) spreading codes, are the in-phase and quadrature-phase components of the lower sideband, and similarly, $c_{UI}(k)$ and $c_{UQ}(k)$ are the in-phase and quadrature-phase components of the upper sideband. $\chi\left(t,f_s^k\right)$ denotes a frequency-hopping subcarrier symbol; T_c is the spreading code chip duration; f_s^k is the subcarrier frequency that corresponds to the k-th spreading code chip; and $*$ denotes the conjugation operator. Typically, $\chi\left(t,f_s^k\right)$ can be defined as follows:

$$\chi\left(t,f_s^k\right)=\begin{cases}\frac{1}{\sqrt{2}}\text{sign}(\cos 2\pi f_s^k t)\\ +j\frac{1}{\sqrt{2}}\text{sign}(\sin 2\pi f_s^k t),\ 0\le t\le T_c\\ 0,\ \text{otherwise}\end{cases} \quad (2)$$

An FH-AltBOC signal can be denoted by FH-AltBOC $(f_h^{M-1}:f_d:f_h^0,f_c)$, where $\{f_h^0:f_d:f_h^{M-1}\}$ is the hopset, which inludes M possible single subcarrier frequencies $\{f_h^0,f_h^1,\ldots,f_h^{M-1}\}$. The hopset is a monotonically increasing arithmetic sequence; $f_d=f_h^i-f_h^{i-1}$, $i=1,2,\ldots,M-1$ is the common difference, i.e., the minimum frequency-hopping interval, and $f_c=1/T_c$ is the spreading code chip rate. Moreover, additional parameters are needed to describe the FH-AltBOC signal, such as the hopping rate, the frequency-hopping pattern, and the frequency-hopping band. The hopping rate is denoted by f_v, and f_c should be an integer multiple of f_v; the frequency-hopping pattern, which is denoted by C_k, is a decimal sequence that controls the frequency hopping of the FH-AltBOC subcarrier; and the frequency-hopping band,

which is denoted by B_s, is sufficiently large for the inclusion of M frequency channels and is defined by $B_s = M \times f_d$. Consistent with the notation of AltBOC signal, the abbreviation FH-AltBOC($\alpha_{M-1} : d : \alpha_0, \beta$) is defined to denote the FH-AltBOC signal as follows:

$$\begin{cases} f_h^{M-1} = \alpha_{M-1} \times f_0 \\ f_d = d \times f_0 \\ f_h^0 = \alpha_0 \times f_0 \\ f_c = \beta \times f_0 \end{cases} \tag{3}$$

where f_0 denotes the reference frequency, which is typically equal to 1.023 MHz. The parameters should satisfy the definition of FH-AltBOC modulation; they must be positive integers, and α_i, $i = 0, 1, 2, \ldots, M-1$ should be an integer multiple of β. Considering all the constraints, the time-domain expression of the nonconstant-envelope FH-BOC signal can be simplified to

$$\begin{cases} s(t) = \sum_{k=-\infty}^{+\infty} \left[c_{LI}(k) + jc_{LQ}(k)\right] \chi^*(t - kT_c, f_s^k) \\ \qquad + \left[c_{UI}(k) + jc_{UQ}(k)\right] \chi(t - kT_c, f_s^k) \\ f_h^i = (\alpha_0 + i \times d) \times f_0, \quad i = 0, 1, 2, \ldots, M-1 \\ f_s^k = f_h^{C_k} \end{cases} \tag{4}$$

B. CONSTANT-ENVELOPE FH-AltBOC

AltBOC(kn,n) is a special case of FH-AltBOC modulation in which the hopset of FH-AltBOC includes only a single subcarrier frequency. Thus, FH-AltBOC is a more generalized type of modulation, and the constant-envelope construction methods of an AltBOC signal can also be used to make the envelope of the FH-AltBOC signal constant to enable the use of the HPA at saturation for higher efficiency. In this paper, we derive the mathematical model of the FH-AltBOC signal with a constant envelope according to the method that was proposed by [4]:

$$\begin{aligned} s(t) = \sum_{k=-\infty}^{+\infty} & \left[c_{LI}(k) + jc_{LQ}(k)\right] \chi_d^*(t - kT_c, f_s^k) \\ & + \left[c_{UI}(k) + jc_{UQ}(k)\right] \chi_d(t - kT_c, f_s^k) \\ & + \left[\bar{c}_{LI}(k) + j\bar{c}_{LQ}(k)\right] \chi_p^*(t - kT_c, f_s^k) \\ & + \left[\bar{c}_{UI}(k) + j\bar{c}_{UQ}(k)\right] \chi_p(t - kT_c, f_s^k) \end{aligned} \tag{5}$$

with

$$\begin{cases} \bar{c}_{LI}(k) = c_{UQ}(k)\, c_{UI}(k)\, c_{LQ}(k) \\ \bar{c}_{LQ}(k) = c_{UI}(k)\, c_{UQ}(k)\, c_{LI}(k) \\ \bar{c}_{UI}(k) = c_{LI}(k)\, c_{UQ}(k)\, c_{LQ}(k) \\ \bar{c}_{UQ}(k) = c_{UI}(k)\, c_{LI}(k)\, c_{LQ}(k) \end{cases} \tag{6}$$

where $\chi_d(t, f_s^k) = 1/2\sqrt{2}[sc_d(t, f_s^k) + jsc_d(t - T_s/4, f_s^k)]$, $\chi_p(t, f_s^k) = 1/2\sqrt{2}[sc_p(t, f_s^k) + jsc_p(t - T_s/4, f_s^k)]$. $sc_d(t, f_s^k)$ and $sc_p(t, f_s^k)$ are subcarrier symbols that are defined as

$$\begin{aligned} & sc_d\left(t, f_s^k\right) \\ & = \begin{cases} \frac{\sqrt{2}}{4}\mathrm{sign}\left[\cos\left(2\pi f_s^k t - \frac{\pi}{4}\right)\right] + \\ \frac{1}{2}\mathrm{sign}\left[\cos\left(2\pi f_s^k t\right)\right] \\ + \frac{\sqrt{2}}{4}\mathrm{sign}\left[\cos\left(2\pi f_s^k t + \frac{\pi}{4}\right)\right], 0 \le t \le T \\ 0, \text{ others} \end{cases} \\ & sc_d\left(t, f_s^k\right) \\ & = \begin{cases} -\frac{\sqrt{2}}{4}\mathrm{sign}\left[\cos\left(2\pi f_s^k t - \frac{\pi}{4}\right)\right] \\ + \frac{1}{2}\mathrm{sign}\left[\cos\left(2\pi f_s^k t\right)\right] \\ - \frac{\sqrt{2}}{4}\mathrm{sign}\left[\cos\left(2\pi f_s^k t + \frac{\pi}{4}\right)\right], 0 \le t \le T \\ 0, \text{ others} \end{cases} \end{aligned} \tag{7}$$

Fig. 1 shows example waveforms of $sc_d\left(t, f_s^k\right)$ and $sc_p\left(t, f_s^k\right)$ for a constant-envelope FH-AltBOC signal, which illustrates how the subcarrier wave changes with the hopping of the frequency-hopping pattern. The left panel of Fig. 2 shows the modulation constellation of a nonconstant-envelope FH-AltBOC signal. The envelope is not constant. The right panel of Fig. 2 shows the modulation constellation of a constant-envelope FH-AltBOC signal. The envelope becomes constant similar to a constant-envelope AltBOC signal.

C. ACF AND PSD

The ACF of the nonconstant-envelope FH-AltBOC signal can be expressed as

$$\begin{aligned} R(t, t+\tau) &= E\left[s(t)\, s^*(t+\tau)\right] \\ &= \sum_{k=-\infty}^{+\infty} \sum_{l=-\infty}^{+\infty} \begin{bmatrix} R_{c_{LI}}(l) + R_{c_{LQ}}(l) \\ + R_{c_{UI}}(l) + R_{c_{UQ}}(l) \end{bmatrix} \\ &\quad \times E\begin{bmatrix} \chi\left(t - kT_c, f_s^k\right) \\ \times \chi^*\left(t + \tau - kT_c - lT_c, f_s^{k+l}\right) \end{bmatrix} \end{aligned} \tag{8}$$

where $R_i(l) = E\left[c_i(k)\, c_i(k+l)\right]$, for $i \in \{LI, LQ, UI, UQ\}$, denote the ACFs of the spreading codes. An ideal spreading code is infinite, aperiodic, independent, and random; thus, $R_i(l) = 1$, $l = 0$, $R_i(l) = 0$, and $l \neq 0$. Therefore, (8) can be simplified to

$$R(t, t+\tau) = 4 \times \sum_{k=-\infty}^{+\infty} E\begin{bmatrix} \chi\left(t - kT_c, f_s^k\right) \\ \times \chi^*\left(t + \tau - kT_c, f_s^k\right) \end{bmatrix} \tag{9}$$

For an FH-AltBOC signal, the probability that a frequency channel is used can be expressed as

$$P\left(f_s^k = f_h^i\right) = \frac{l_i}{L_c}, \quad i = 0, 1, 2, \ldots, M-1 \tag{10}$$

where L_c denotes the total number of occurrences of all frequency channels and l_i denotes the number of occurrences

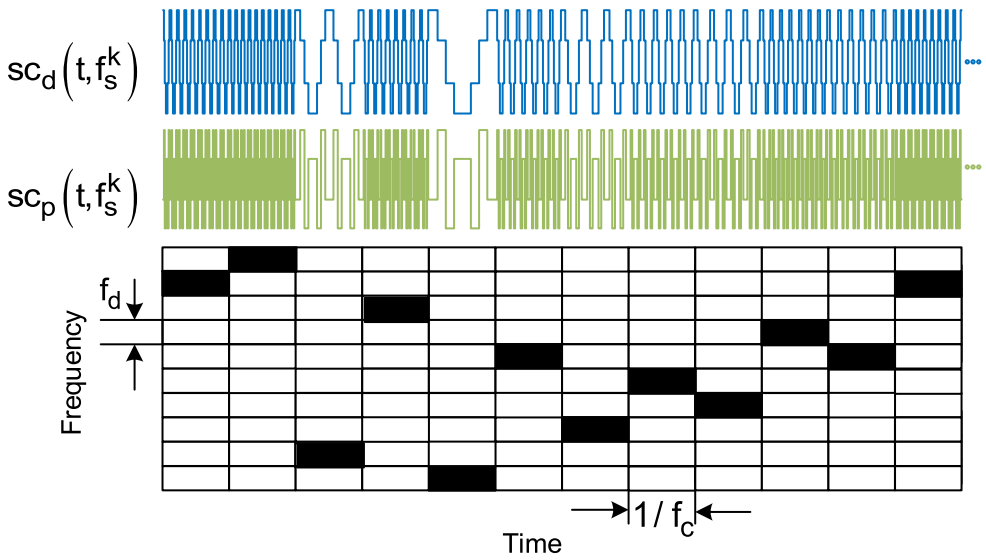

FIGURE 1. Waveforms of $sc_d\left(t, f_s^k\right)$ and $sc_p\left(t, f_s^k\right)$ for a constant-envelope FH-AltBOC signal.

of the channel f_h^i. Therefore, by substituting (10) into (9), $R(t, t+\tau)$ can be simplified to

$$R(t,t+\tau)=\frac{4}{L_c}\sum_{k=-\infty}^{+\infty}\sum_{i=0}^{M-1}\chi\left(t-kT_c,f_h^i\right)\times\chi^*\left(t+\tau-kT_c,f_h^i\right)\times l_i \quad (11)$$

The FH-AltBOC signal is not a wide-sense stationary process but rather has the following characteristics:

$$\begin{aligned}E\left[s\left(t+T_c\right)\right]&=E\left[s\left(t\right)\right]\\ R\left(t+T_c,t+\tau+T_c\right)&=R\left(t,t+\tau\right)\end{aligned} \quad (12)$$

Thus, this signal is cyclostationary, and its ACF that depends on only τ can be obtained by averaging the ACF over the interval $t\in[0,T_c]$:

$$R(\tau)=\frac{1}{T_c}\int_0^{T_c}R\left(t,t+\tau\right)dt \quad (13)$$

The detailed derivation of $R(\tau)$ for the nonconstant-envelope and the constant-envelope FH-AltBOC signals can be found in the appendix. For the nonconstant-envelope FH-AltBOC signal, the normalized ACF, $R_{\mathrm{NCE}}(\tau)$,is

$$\begin{aligned}R_{\mathrm{NCE}}(\tau)=\frac{1}{L_cT_c}\sum_{i=0}^{M-1}l_iT_h^i\Bigg\{&2\sum_{m=0}^{N_i-1}\sum_{n=0}^{N_i-1}(-1)^{m+n+1}\\&\times\Lambda_{T_h^i}\left[\tau-\left(m+n+1-N_i\right)T_h^i\right]\\&+\sum_{m=0}^{2N_i-1}\sum_{n=0}^{2N_i-1}(-1)^{\lfloor\frac{m+1}{2}\rfloor+\lfloor\frac{n+1}{2}\rfloor}\\&\times\Lambda_{T_h^i/2}\left[\tau-\left(m+n+1-2N_i\right)\frac{T_h^i}{2}\right]\Bigg\}\end{aligned} \quad (14)$$

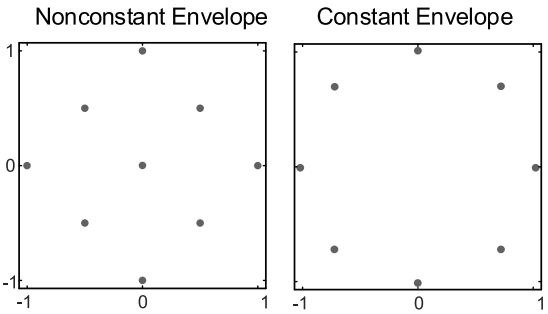

FIGURE 2. Modulation constellations of FH-AltBOC modulation.

where $N_i=2\alpha_i/\beta$ and $\Lambda_{T_h^i}(\tau)$ is the triangle function with support $2T_h^i$, where $T_h^i=0.5\left(f_h^i\right)^{-1}$, which is defined as

$$\Lambda_{T_h^i}(\tau)=\begin{cases}1-\dfrac{|\tau|}{T_h^i}, & |\tau|\le T_h^i\\ 0, & \text{otherwise}\end{cases} \quad (15)$$

For the constant-envelope FH-AltBOC signal, the normalized ACF, $R_{\mathrm{CE}}(\tau)$, is

$$\begin{aligned}R_{\mathrm{CE}}(\tau)=\frac{1}{L_cT_c}\sum_{i=0}^{M-1}\sum_{m=0}^{4N_i-1}\sum_{n=0}^{4N_i-1}l_iT_h^i\Bigg[&\frac{1}{16}(-1)^{\lfloor\frac{m}{4}\rfloor+\lfloor\frac{n}{4}\rfloor+1}\\&+\frac{1}{16}(-1)^{\lfloor\frac{m+2}{4}\rfloor+\lfloor\frac{n+2}{4}\rfloor}+\frac{1}{8}(-1)^{\lfloor\frac{m+1}{4}\rfloor+\lfloor\frac{n+3}{4}\rfloor}\Bigg]\\&\times\Lambda_{T_h^i/4}\left[\tau-\left(m+n+1-4N_i\right)\frac{T_h^i}{4}\right]\end{aligned} \quad (16)$$

where $\lfloor\cdot\rfloor$ denotes the floor function.

According to the Wiener–Khinchin theorem [20], the PSD of $s(t)$ is the Fourier transform of its ACF, i.e., $G(f)=\mathrm{FT}[R(\tau)]$. By substituting (14) into it, the PSD of the

nonconstant-envelope FH-AltBOC signal can be derived as follows:

$$G_{\mathrm{NCE}}(f)=\frac{2}{L_cT_c}\sum_{i=0}^{M-1}l_i\left\{\frac{\sin^2\left(\pi fT_h^i\right)\sin^2\left(\pi fT_c\right)}{\pi^2f^2\cos^2\left(\pi fT_h^i\right)}+\frac{\left[1-\cos\left(\pi fT_h^i\right)\right]^2\sin^2\left(\pi fT_c\right)}{\pi^2f^2\cos^2\left(\pi fT_h^i\right)}\right\} \tag{17}$$

Similarly, the PSD of the constant-envelope FH-AltBOC signal can be derived as follows:

$$G_{\mathrm{CE}}(f)=\frac{1}{L_cT_c}\sum_{i=0}^{M-1}l_i\left\{\frac{\sin^2\left(\pi fT_c\right)\sin^2\left(\pi f\frac{T_h^i}{4}\right)}{\pi^2f^2\cos^2\left(\pi fT_h^i\right)}\times\left[4\cos^2\left(\pi f\frac{T_h^i}{4}\right)+2\sin\left(\pi fT_h^i\right)\sin\left(\pi f\frac{T_h^i}{2}\right)+2\right]\right\} \tag{18}$$

The frequency hopping of the FH-AltBOC subcarrier determines the similarities and differences in terms of the ACF and PSD between FH-AltBOC and AltBOC modulations. It potentially endows the signal with various excellent properties, such as low ACF ambiguity and better anti-interception and anti-narrowband interference performance.

For an FHSS system, a uniformly distributed frequency-hopping pattern and a larger hopping rate yield better anti-interception and anti-narrowband interference performance [18]; thus, we only discuss FH-BOC signals with a uniform subcarrier and a hopping rate equal to the spreading code chip rate. The zero-crossing nearest the ACF main peak (ZCNM) for an FH-AltBOC signal can be expressed as

$$\tau_{\mathrm{ZCNM}}=\min\left\{\tau\,|R(\tau)=0,\tau>0\right\} \tag{19}$$

and the ACF main peak width is twice the time delay τ_{ZCNM}. A narrower ACF main peak may provide higher code tracking accuracy. The ACF main-peak-to-maximum-side-peak ratio (MSR) can be calculated as

$$R_{\mathrm{MSR}}=20\lg\left(\max_{|\tau|>\tau_{\mathrm{ZCNM}}}|R(\tau)|\right) \tag{20}$$

where $|\cdot|$ denotes the absolute value operator. A lower MSR can mitigate the ACF peak ambiguity [21]. Moreover, the PSD main-lobe bandwidth (MLB) for the FH-AltBOC signal is defined as the bandwidth that contains the two split spectral lobes and is approximately $2\left(\alpha_{M-1}+\beta\right)\times f_0$. A larger MLB may yield higher code tracking accuracy and better anti-interception and anti-narrowband interference performance. The maximum value of the PSD (MVP) for the FH-AltBOC signal is defined as

$$m_{\mathrm{MVP}}=\max_{f\in\mathrm{MLB}}G(f) \tag{21}$$

A smaller MVP enables higher power signal transmission without increasing the interference from the noise floor, which is more conducive to self-spectral separation [22].

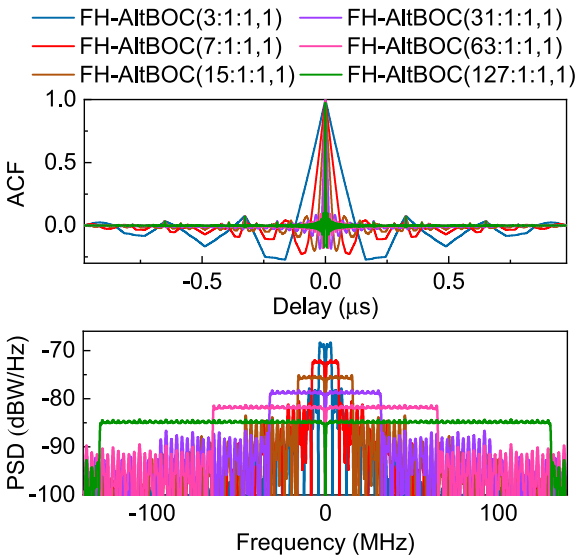

FIGURE 3. Normalized ACFs and PSDs for FH-AltBOC (α_{M-1}:1:1,1) signals.

FH-AltBOC modulation is an extensive modulation family, which provides four parameters, a frequency-hopping pattern, and a hopping rate via which designers can shape the ACF and PSD; the optimal values will be differ among constraint criteria. In this paper, we propose FH-AltBOC(α_{M-1}:1:1,1), in which the minimum frequency-hopping interval, the minimum subcarrier frequency, and the spreading code chip rate are fixed to their minimum possible values; the frequency-hopping pattern is assumed to be uniformly distributed; and the hopping rate is fixed to its maximum possible value, i.e., equal to the spreading code chip rate. The reasons for recommending FH-AltBOC(α_{M-1}:1:1,1) signals are that they have the most subcarrier frequencies, the largest MLB, and the flattest spectral shape, which yield the best anti-interception and anti-narrowband interference performance; a uniformly distributed frequency-hopping pattern and a larger hopping rate yield better anti-interception and anti-narrowband interference performance. The top panel of Fig. 3 shows a set of ACFs for FH-AltBOC(α_{M-1}:1:1,1) signals; panels (a) and (c) of Fig. 4 plot the ZCNM and MSR, respectively, versus the maximum subcarrier frequency. The larger the maximum subcarrier frequency is, the smaller the ZCNM and the larger the MSR. The bottom panel of Fig. 3 shows a set of PSDs of FH-AltBOC(α_{M-1}:1:1,1) signals. The larger the maximum subcarrier frequency is, the smaller the MVP and the flatter the spectral shape.

If better spectral separation with signals at the center of the band is needed, FH-AltBOC(α_{M-1}:1:α_0,1), where $\alpha_0>1$, is proposed. By increasing the minimum subcarrier frequency α_0, the signal power will be moved away from the band center, and the ACF main peak will be narrowed, thereby potentially improving the code tracking accuracy. The top panel of Fig. 5 shows a set of ACFs for FH-AltBOC(64:1:α_0,1)

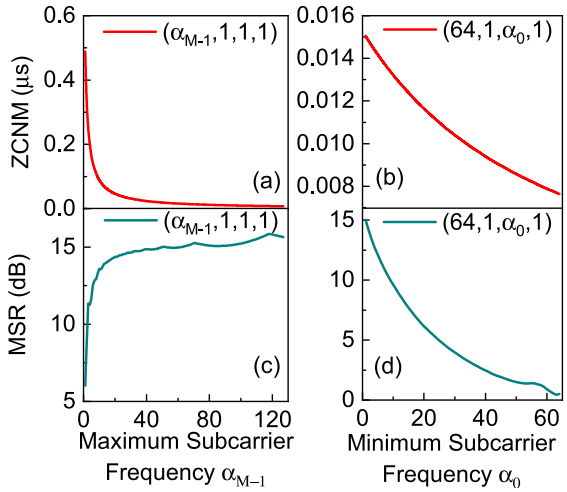

FIGURE 4. ZCNMs and MSRs for FH-AltBOC(α_{M-1}:1:1,1) and FH-AltBOC(64:1:α_0,1) signals.

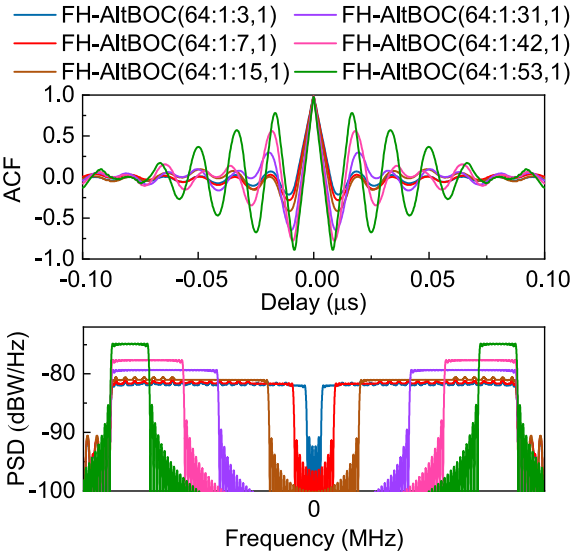

FIGURE 5. Normalized ACFs and PSDs for FH-AltBOC(64:1:α_0,1) signals.

signals; panels (b) and (d) of Fig. 4 plot the ZCNM and MSR, respectively, versus the minimum subcarrier frequency. The larger the minimum subcarrier frequency is, the smaller the ZCNM and the MSR. The bottom panel of Fig. 5 shows a set of PSDs of FH-AltBOC(64:1:α_0,1) signals. The larger the minimum subcarrier frequency is, the larger the MVP and the farther the signal power moves away from the band center.

D. GENERATION AND DETECTION SCHEME

The FH-AltBOC subcarrier is generated by combining several square waves, which can be digitally implemented and processed by a software-defined receiver. Thus, the subcarrier frequency can be switched instantaneously, thereby, overcoming the shortcomings of a frequency synthesizer during frequency switching. The performance for carrier-phase measurements and Doppler measurement with the FH-AltBOC signal are not affected relative to that with AltBOC signals because the frequency hopping is implemented in the baseband. Fig. 6 shows the architecture of a direct computation method for the FH-AltBOC signal generation. The data, spreading code, subcarrier, and RF carrier should be generated from a common clock so that they have constant phase offsets.

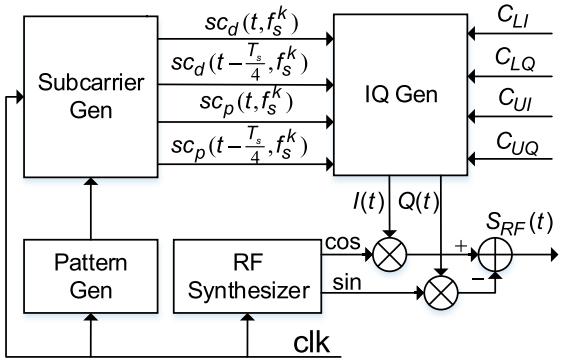

FIGURE 6. Block diagram of FH-AltBOC signal generation.

Fig. 7 shows a serial search direct acquisition scheme for the FH-AltBOC signal. First, the RF signal $S_{RF}(t)$ was mixed with the local oscillator signal, down-converted to an intermediate frequency (IF) signal $S_{IF}(t)$; then, the IF signal $S_{IF}(t)$ is down-converted by the local carrier and cross-correlated by the local reference signal, respectively; next, after coherent integrations and square operation, the decision variable can be obtained by adding the outputs of I and Q channels:

$$S_D = S_I^2 + S_Q^2 \tag{22}$$

where S_I and S_Q are the outputs of the I and Q channels, respectively. S_D is the chi-square random variable with two degrees of freedom. The acquisition threshold $V_T = -2\sigma^2 \ln P_{fa}$ can be calculated from the noise variance σ^2 and the desired probability of false alarm P_{fa} [23]. Conventional GNSS signal acquisition algorithms are two-dimensional search processes of the code dimension and the Doppler dimension. However, The FH-AltBOC signal acquisition has an additional search dimension—the frequency-hopping dimension. Thus, the frequency-hopping pattern has a substantial effect on the acquisition time and acquisition complexity of the FH-AltBOC signal. For military signals, a pseudorandom frequency-hopping pattern with a large period is recommended, which is difficult for a noncooperative receiver to reproduce and dehop. However, when the period of the frequency-hopping pattern is large, the signal acquisition time and acquisition complexity increase, thereby requiring a higher performance receiver. To eliminate this limitation, we present a frequency-hopping scheme in which the hopping rate f_v and the period of the frequency-hopping pattern are adjusted. Let f_v be equal to f_c and the period of the frequency-hopping pattern be an integer multiple of the spreading code period. The phase of the frequency-hopping pattern can be

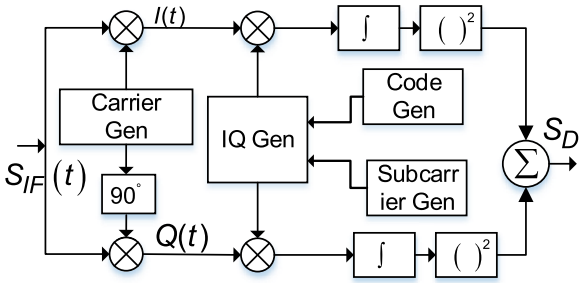

FIGURE 7. Block diagram of FH-AltBOC signal detection.

derived from the spreading code phase since they have a constant phase offset. Thus, we can significantly narrow the search space, and the average acquisition time can be estimated as

$$T_{acq} = \frac{1}{2}\frac{f_{unc}t_{unc}N_T T_{dwell}}{f_{bin}t_{bin}} \tag{23}$$

where f_{unc} and t_{unc} denote the Doppler frequency uncertainty and the spreading code phased uncertainty, respectively; f_{bin} and t_{bin} denote the Doppler frequency bin and the spreading code bin, respectively, where each search increment is a bin; N_T is the ratio of the period of the frequency-hopping pattern and the spreading code period; and T_{dwell} is the search dwell time. The acquisition time and acquisition complexity of the FH-AltBOC signal will be the same as those of the AltBOC signal with the same MLB if the period of the frequency-hopping pattern is equal to the spreading code period. An AltBOC receiver can process such a signal with only minor modifications.

For example, Let f_v be equal to f_c, the lengths of the spreading code and the frequency-hopping pattern be 1023. For constant-envelope FH-AltBOC(24:1:1,1) and FH-AltBOC(24:1:6,1) signals that are generated via this scheme, the simulated and theoretical normalized ACF results are compared in the top panel of Fig. 8, and the simulated and theoretical PSD results are compared in the bottom panel. Consider a receiver front-end bandwidth of 60 MHz, a sampling rate of 173 MHz, an IF of 36 MHz, a carrier-to-noise-density ratio (C/N_0) of 45 dB, an early-late spacing of 11.6 ns, and a coherent integration time of 1 ms, Fig. 9 shows the output of FH-AltBOC(24:1:1,1) from the serial search direct acquisition scheme; the code phase and frequency-hopping pattern are 450 chips and the carrier frequency is 36 MHz.

III. PERFORMANCE ANALYSIS

This section focuses on the performance of several representative constant-envelope FH-AltBOC signals in comparison with AltBOC signals. These signals are FH-AltBOC(24:1:1,1), FH-AltBOC(24:1:6,1), AltBOC(12,1), and AltBOC(15,10). AltBOC(15,10) has been adopted for the Galileo E5 signal [4]. FH-AltBOC(24:1:1,1) has the same MLB as AltBOC(15,10), and its ZCNM is approximately equal to that of AltBOC(12,1); FH-AltBOC(24:1:6,1)

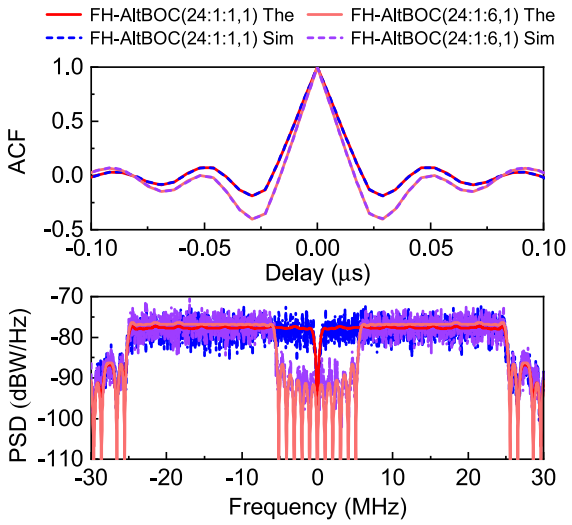

FIGURE 8. Simulated and theoretical results of the normalized ACFs and PSDs for the example signals.

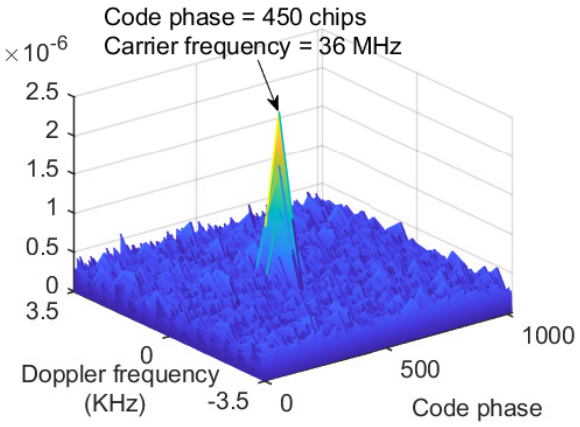

FIGURE 9. Output from serial search acquisition for FH-AltBOC(24:1:1,1).

has the same MLB and ZCNM as AltBOC(15,10). Since FH-AltBOC(24:1:1,1), FH-AltBOC(24:1:6,1), and AltBOC(15,10) have the same MLB, they can be processed by receivers with the same front-end bandwidth, i.e., the same receiving complexity. We discuss the properties of the ACFs and PSDs, the probabilities of false locking on ACF side peaks, the code tracking performance, and the anti-narrowband interference and multipath performance for the example signals.

A. COMPARISON OF ACFs AND PSDs

Fig. 10 depicts the ACFs and PSDs for the example signals computed over an infinite bandwidth, and various properties of the ACFs and PSDs are listed in Table 1. The MSR of FH-AltBOC(24:1:1,1) is the largest among the example signals, and the MSR of FH-AltBOC(24:1:6,1) is larger than that of AltBOC(15,10). The ZCNMs of FH-AltBOC(24:1:6,1) and AltBOC(15,10) are the smallest among the example signals.

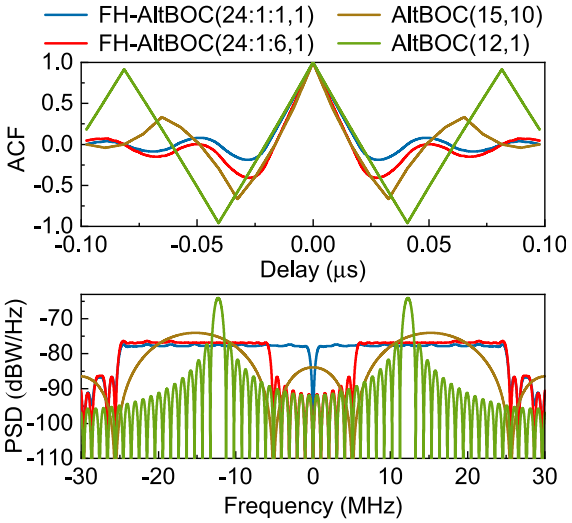

FIGURE 10. Normalized ACFs and PSDs for the example signals.

TABLE 1. ACF and PSD properties of the example signals.

Property	ZCNM (ns)	MSR (dB)	MLB (MHz)	MVP (dBW/Hz)
FH-AltBOC (24:1:1,1)	19.6	14.5	51.2	-77.2
FH-AltBOC (24:1:6,1)	16.3	7.8	51.2	-76.4
AltBOC (15,10)	16.3	3.6	51.2	-74.0
AltBOC (12,1)	20.4	0.5	26.6	-64.0

The ZCNM of FH-AltBOC(24:1:1,1) is slightly smaller than that of AltBOC(12,1). The PSD main lobes of FH-AltBOC(24:1:6,1), AltBOC(15,10), and AltBOC(12,1) are offset from the band center but that of AltBOC(24:1:1,1) is evenly distributed within the band except for depression in the band center. The MVP of FH-AltBOC(24:1:1,1) is the smallest among the example signals, and the MVP of FH-AltBOC(24:1:6,1) is smaller than that of AltBOC(15,10).

Suppose that the signals are bandlimited to 60 MHz at the transmitter. Fig. 11 plots the signal power percentages versus the front-end bandwidth of the receiver β_r, according to which the minimum bandwidths must contain a sufficient amount of power for the example signals. When β_r is larger than 50 MHz, almost 100-percent power is contained for the example signals.

B. PROBABILITIES OF FALSE LOCKING ON ACF SIDE PEAKS

By comparing the ACFs for the example signals, we observe that the ACF side peaks for the FH-AltBOC signals are much lower than for the AltBOC signals, thereby substancially mitigating the ACF peak ambiguity. To explore the ACF peak ambiguity for the example signals during the serial search direct acquisition, we conduct a Monte Carlo simulation with 10000 runs. For a receiver front-end bandwidth of 60 MHz,

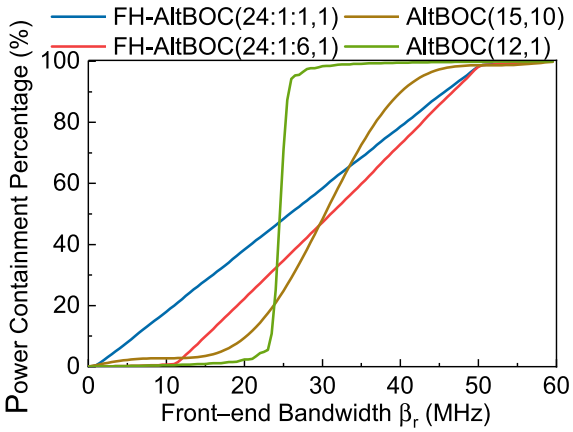

FIGURE 11. Power containment percentages for the example signals.

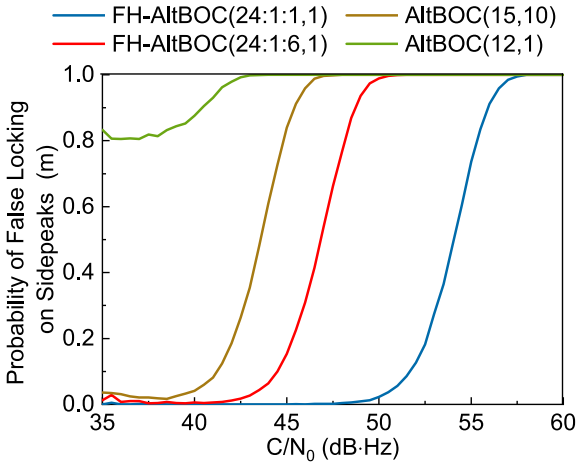

FIGURE 12. Probabilities of false locking on ACF side peaks for the example signals.

a sampling rate of 173 MHz, an IF of 36 MHz, an early-late spacing of 11.6 ns, and a coherent integration time of 1 ms, Fig. 12 shows the simulated probabilities of false locking on ACF side peaks for the example signals. The false locking probabilities increase with (C/N_0) because the amplitudes of the ACF side peaks also increase simultaneously. FH-AltBOC(24:1:1,1) has the smallest false locking probability among the example signals, whereas AltBOC(12,1) has the largest. FH-AltBOC(24:1:6,1) has smaller false locking probability than AltBOC(15,10).

C. CODE TRACKING ACCURACY

The signal modulation scheme determines the ultimate code tracking accuracy. With the development of receiver processing technology, the signal modulation scheme has become the main factor that limits the code tracking performance. We compare the ultimate code tracking performance for the example signals.

1) ROOT MEAN SQUARE (RMS) BANDWIDTH

The RMS bandwidth of a bandlimited signal is defined in [21]. The larger the RMS bandwidth is, the lower the bound

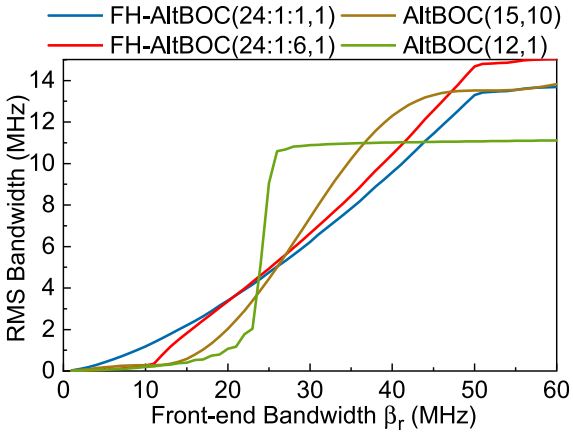

FIGURE 13. RMS bandwidths for the example signals.

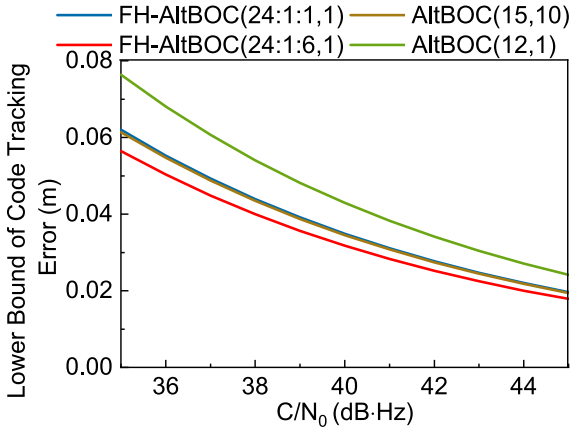

FIGURE 14. Lower bounds of the code tracking error for the example signals.

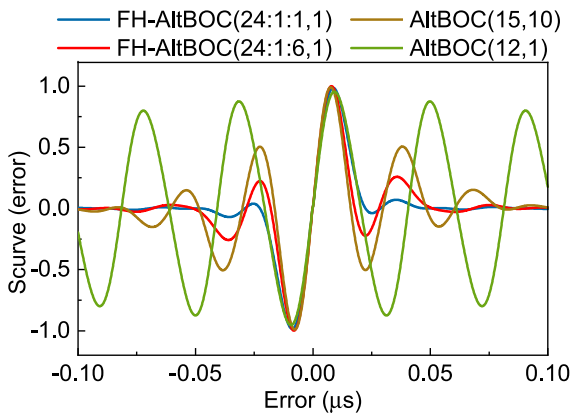

FIGURE 15. S-curves for the example signals.

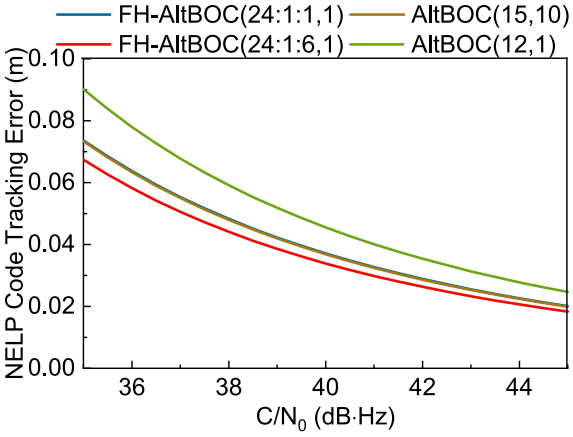

FIGURE 16. NELP code tracking errors for the example signals.

on the code tracking accuracy. Fig. 13 plots the RMS bandwidths of the example signals as functions of the front-end bandwidth. When the front-end bandwidth β_r is equal to 60 MHz, The β_{rms} of FH-AltBOC(24:1:6,1) is the largest, the β_{rms} of FH-AltBOC(24:1:1,1) and AltBOC(15,10) are almost equal, and the β_{rms} of AltBOC(12,1) is the smallest among the example signals.

2) LOWER BOUND OF THE CODE TRACKING ERROR

A lower bound of the code tracking error is independent of the code tracking method and reflects the ultimate tracking performance [24]. For an equivalent rectangular bandwidth of the code tracking loop of 1 Hz, an integration time of 1 ms, and a front-end bandwidth of 60 MHz, Fig. 14 shows the lower bounds of the code tracking error for the example signals versus C/N_0. The lower bound of FH-AltBOC(24:1:6,1) is the smallest, the lower bounds of FH-AltBOC(24:1:1,1) and AltBOC(15,10) are almost equal, and the lower bound of AltBOC(12,1) is the largest among the example signals.

D. PERFORMANCE OF NONCOHERENT EARLY-LATE PROCESSING

The ACF for the FH-AltBOC signal has a symmetric peak, which is similar to that for the AltBOC signal. Thus, code tracking with the FH-AltBOC signal can rely on a discriminator based on conventional early-late processing. This subsection shows noncoherent early-late processing (NELP) for the example signals.

The S-curve produced by a NELP-based discriminator with an early-late spacing of D seconds is expressed in [21] as follows:

$$S(\varepsilon) = \left|R\left(\varepsilon - \frac{D}{2}\right)\right|^2 - \left|R\left(\varepsilon + \frac{D}{2}\right)\right|^2 \tag{24}$$

where ε is the error in the signal arrival time and $R(\tau)$ is the normalized ACF for the signal.

For an early-late spacing of 16 ns, a front-end bandwidth of 60 MHz. Fig. 15 shows the S-curves for the example signals. The S-curve side peaks near the false locking points for FH-AltBOC(24:1:1,1) are the lowest among the example signals; hence, the ambiguity problem in code tracking is mitigated.

The variance of the code tracking error for NELP in white noise is specified in [25]. For an interference power of zero, a front-end bandwidth of 60 MHz, an integration time of 1 ms, an early-late spacing of 16 ns, and a one-side equivalent rectangular bandwidth of the code tracking loop of 1 Hz,

TABLE 2. Processing gains for the example signals.

Parameter	FH-AltBOC (24:1:1,1)	FH-AltBOC (24:1:6,1)	AltBOC (15,10)	AltBOC (12,1)
G_p(dB)	59.9	58.9	56.1	46.1

the code tracking errors for the example signals versus C/N_0 are compared in Fig. 16. The NELP comparison results for the example signals are consistent with the lower bounds of the code tracking error.

E. ANTI-NARROWBAND INTERFERENCE PERFORMANCE

The DSSS technique employed by GNSS signals offers strong anti-interference performance. However, GNSS signals are weak, easily suffering from interference. A modulation scheme with better anti-interference performance could improve signal tracking performance. We compare the anti-interference performance for the narrowband interference for the example signals. For a spread spectrum system, the processing gain can reflect the anti-interference performance, especially for narrowband interference. A larger processing gain corresponds to better anti-interference performance [26]. The processing gain for AltBOC(α,β) can be expressed as

$$G_{\text{AltBOC}} \approx 10\lg\left(\beta \times \frac{f_0}{f_D}\right) + 3 \tag{25}$$

and the processing gain for FH-AltBOC(α_{M-1}:1 :α_0, β) is

$$G_{\text{FH-AltBOC}} \approx 10\lg\left(\beta \times \frac{f_0}{f_D}\right) + 10\lg\left(\frac{\alpha_{M-1} - \alpha_0}{\beta} + 1\right) + 3 \tag{26}$$

The comparison of (25) and (26) reveals that the processing gain for FH-AltBOC(α_{M-1}:1 :α_0, β) is 10lg [$(\alpha_{M-1} - \alpha_0)/\beta$ + 1] dB higher than that for AltBOC(α,β); hence, FH-BOC modulation offers better anti-narrowband interference performance than the equivalent AltBOC modulation. Table 2 lists the processing gains for the example signals. FH-AltBOC(24:1:1,1) has the largest processing gain, and AltBOC(12,1) has the smallest. The processing gain for FH-AltBOC(24:1:6,1) is 2.8 dB higher than that for AltBOC(15,10).

The effect of interference on a receiver can be measured in terms of the effective carrier-power-to-noise ratio, which is defined in [24]. For a front-end bandwidth of 60 MHz, C/N_0 of 45 dB, narrowband interference with a bandwidth of 10 KHz, and the center frequency located at the center of one of the main lobes of the signal, Fig. 17 plots the effective C/N_0 versus jammer-to-noise ratio (C_I/N_0) for the example signals. The differences in the processing gains for the example signals are readily observed in Fig. 17.

F. MULTIPATH PERFORMANCE

Multipath interference is one of the main sources of error in satellite navigation [27]. For a multipath scenario with one

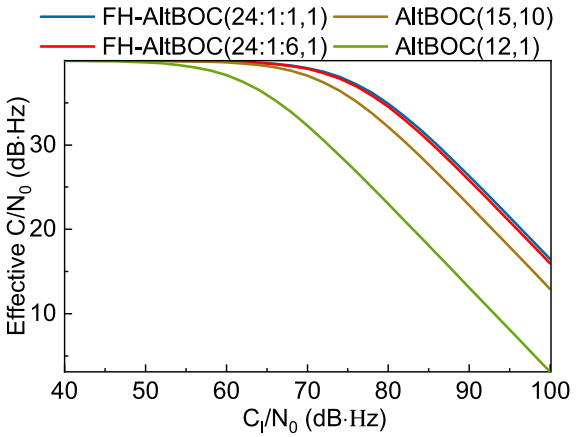

FIGURE 17. Effective C/N_0 values for the example signals.

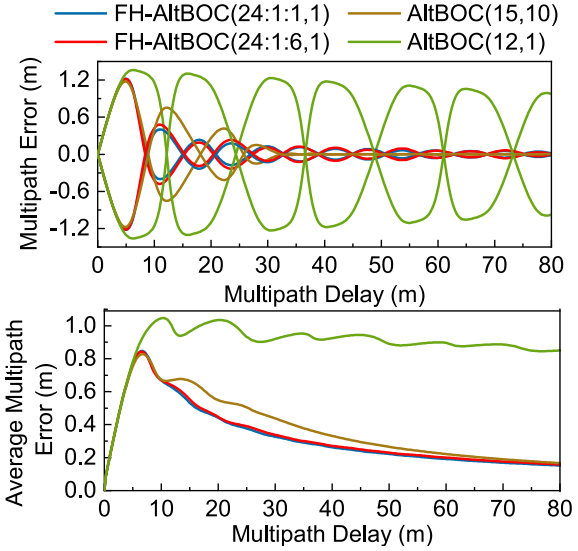

FIGURE 18. NELP multipath errors for the example signals.

direct path and one reflected path with a multipath-to-direct ratio of −6 dB, an early-late spacing of 16 ns, and a front-end bandwidths of 60 MHz, the top panel of Fig. 18 plots the NELP multipath error envelopes versus the multipath delay for the example signals, and the bottom panel plots the smallest average multipath error. The error envelopes for FH-AltBOC(24:1:1,1) and FH-AltBOC(24:1:6,1) are smaller than those for AltBOC(15,10) and AltBOC(12,1) when the path delay is less than 30 m, which is the most common path delay in many urban environments [28]. FH-AltBOC(24:1:1,1) has the smallest average multipath error, and AlBOC(12,1) has the largest average multipath error among the example signals. FH-AltBOC(20:1:6,1) has lower average multipath error than AltBOC(15,10).

IV. CONCLUSION

We propose a generalized FH-AltBOC modulation. Based on theoretical and numerical analyses, FH-AltBOC(α_{M-1}:1:1,1)

is recommended due to its lowest ACF ambiguity, best anti-interception, anti-narrowband interference, and multipath performance. FH-AltBOC(α_{M-1}:1:1,1) has better tracking performance than AltBOC(α_{M-1}/2,1), and it can be easily extended to high order with a wider band for better performance. If better spectral separation with signals at the center of the band and higher code tracking accuracy are needed, FH-AltBOC(α_{M-1}:1: α_0,1) with $\alpha_0 > 1$ is recommended, which can provide higher code tracking accuracy and better anti-narrowband interference and multipath performance than AltBOC with the same MLB and ZCNM. FH-AltBOC modulation provides designers with substantial flexibility for adjustment and optimization. If suitable parameters are selected, the acquisition time and acquisition complexity of FH-AltBOC modulation will be the same as those of AltBOC modulation, the generation and detection scheme of FH-AltBOC can be implemented based on that of AltBOC with minor modifications.

FH-AltBOC modulation inherits the advantages of AltBOC modulation, and the constant-envelope construction methods for AltBOC are also applicable for FH-AltBOC. Furthermore, FH-AltBOC modulation enables more multiple accesses than AltBOC modulation with the same spreading code because it has a two-dimensional multiple-access space. The proposed modulation scheme can serve as a new paradigm of signal design for next-generation GNSS and GNSS-like systems, such as systems for indoor positioning, GNSS enhancement, and pseudolite-based positioning.

APPENDIX A
ACF FOR FH-ALTBOC MODULATION

Substituting (11) into (13), the ACF for the nonconstant-envelope FH-AltBOC signal can be expressed as

$$R_{\mathrm{NCE}}(\tau) = \frac{4}{L_c T_c}\int_0^{T_c}\sum_{k=-\infty}^{+\infty}\sum_{i=0}^{M-1}\chi\left(t-kT_c,f_h^i\right) \times\chi^*\left(t+\tau-kT_c,f_h^i\right)\times l_i dt \quad (27)$$

Let $t' = t - kT_c$ and substitute it into (27). The expression of $R(\tau)$ becomes

$$\begin{aligned} R_{\mathrm{NCE}}(\tau) &= \frac{4}{L_c T_c}\sum_{k=-\infty}^{+\infty}\int_{-kT_c}^{(1-k)T_c}\sum_{i=0}^{M-1}\chi\left(t',f_h^i\right) \times\chi^*\left(t'+\tau,f_h^i\right)\times l_i dt \\ &= \frac{4}{L_c T_c}\int_{-\infty}^{+\infty}\sum_{i=0}^{M-1}\chi\left(t',f_h^i\right)\chi^*\left(t'+\tau,f_h^i\right)\times l_i dt \\ &= \frac{4}{L_c T_c}\sum_{i=0}^{M-1}\left[R^i_{p_{\sin}}(\tau)+R^i_{p_{\cos}}(\tau)\right]\times l_i \end{aligned} \quad (28)$$

where $R^i_{p_{\cos}}(\tau)$ and $R^i_{p_{\sin}}(\tau)$ denote the ACFs of the in-phase and quadrature components, respectively, of the frequency-hopping subcarrier symbols defined by (2). $R^i_{p_s}(\tau)$, $s\in\{\sin, \cos\}$ can be expressed as

$$\begin{aligned} R^i_{p_s}(\tau) &= \int_{-\infty}^{+\infty} p_s\left(t,f_h^i\right)p_s^*\left(t+\tau,f_h^i\right)dt \\ &= p_s\left(\tau,f_h^i\right)\otimes p_s^*\left(-\tau,f_h^i\right) \end{aligned} \quad (29)$$

where $\otimes$ denotes the convolution operation and $p_s\left(t,f_h^i\right)$ denotes the symbol of the in-phase or quadrature component. According to the definition, $p_{\sin}\left(t,f_h^i\right)$ has the following property:

$$p_{\sin}\left(t,f_h^i\right) = -p_{\sin}\left(T_c-t,f_h^i\right) \quad (30)$$

Thus, by substituting (30) into (29), $R^i_{p_{\sin}}(\tau)$ can be expressed as

$$\begin{aligned} R^i_{p_{\sin}}(\tau) &= -p_{\sin}\left(\tau,f_h^i\right)\otimes p_{\sin}\left(\tau+T_c,f_h^i\right) \\ &= -p_{\sin}\left(\tau,f_h^i\right)\otimes p_{\sin}\left(\tau,f_h^i\right)\otimes\delta\left(\tau+T_c\right) \end{aligned} \quad (31)$$

where $\delta(\cdot)$ denotes the impulse function. Furthermore, $p_{\sin}\left(\tau,f_h^i\right)$ can also be expressed as

$$p_{\sin}\left(\tau,f_h^i\right) = \frac{1}{\sqrt{2}}\mu_{T_h^i}(\tau)\otimes\sum_{m=0}^{N_i-1}(-1)^m\delta\left(\tau-mT_h^i\right) \quad (32)$$

where $\mu_{T_h^i}(\tau)$ is the rectangular pulse with support T_h^i, which is defined as

$$\mu_{T_h^i}(\tau) = \begin{cases} 1, & 0\le\tau\le T_h^i \\ 0, & \text{otherwise} \end{cases} \quad (33)$$

Next, by substituting (32) into (31), $R^i_{p_{\sin}}(\tau)$ is converted to

$$\begin{aligned} R^i_{p_{\sin}}(\tau) &= \frac{1}{2}\mu_{T_h^i}(\tau)\otimes\sum_{m=0}^{N_i-1}(-1)^m\delta\left(\tau-mT_h^i\right)\otimes\mu_{T_h^i}(\tau) \\ &\quad\otimes\sum_{n=0}^{N_i-1}(-1)^n\delta\left(\tau-nT_h^i\right)\otimes(-1)\delta\left(\tau+T_c\right) \\ &= \frac{1}{2}\sum_{m=0}^{N_i-1}\sum_{n=0}^{N_i-1}(-1)^{m+n+1}T_h^i \\ &\quad\times\Lambda_{T_h^i}\left[\tau-(m+n+1)T_h^i+T_c\right] \\ &= \frac{1}{2}\sum_{m=0}^{N_i-1}\sum_{n=0}^{N_i-1}(-1)^{m+n+1}T_h^i \\ &\quad\times\Lambda_{T_h^i}\left[\tau-(m+n+1-N_i)T_h^i\right] \end{aligned} \quad (34)$$

For $p_{\cos}\left(t,f_h^i\right)$, it has the following property:

$$p_{\cos}\left(t,f_h^i\right) = p_{\cos}\left(T_c-t,f_h^i\right) \quad (35)$$

Thus, by substituting (35) into (29), $R^i_{p_{\cos}}(\tau)$ is converted to

$$\begin{aligned} R^i_{p_{\cos}}(\tau) &= p_{\cos}\left(\tau,f_h^i\right)\otimes p_{\cos}\left(\tau+T_c,f_h^i\right) \\ &= p_{\cos}\left(\tau,f_h^i\right)\otimes p_{\cos}\left(\tau,f_h^i\right)\otimes\delta\left(\tau+T_c\right) \end{aligned} \quad (36)$$

Furthermore, $p_{\cos}\left(\tau, f_h^i\right)$ can also be expressed as

$$p_{\cos}\left(\tau, f_h^i\right) = \mu_{T_h^i/2}(\tau) \otimes \sum_{m=0}^{2N_i-1} (-1)^{\lfloor \frac{m+1}{2} \rfloor} \delta\left(\tau - \frac{mT_h^i}{2}\right) \tag{37}$$

By substituting (37) into (36), $R_{p_{\cos}}^i(\tau)$ is converted to

$$\begin{aligned}
&R_{p_{\cos}}^i(\tau) \\
&= \frac{1}{2}\mu_{T_h^i/2}(\tau) \otimes \sum_{m=0}^{2N_i-1} (-1)^{\lfloor \frac{m+1}{2} \rfloor} \delta\left(\tau - \frac{mT_h^i}{2}\right) \\
&\quad \otimes \mu_{T_h^i/2}(\tau) \sum_{n=0}^{2N_i-1} (-1)^{\lfloor \frac{n+1}{2} \rfloor} \delta\left(\tau - \frac{nT_h^i}{2}\right) \otimes \delta(\tau + T_c) \\
&= \frac{1}{2} \sum_{m=0}^{2N_i-1} \sum_{n=0}^{2N_i-1} (-1)^{\lfloor \frac{m+1}{2} \rfloor + \lfloor \frac{n+1}{2} \rfloor} \frac{T_h^i}{2} \\
&\quad \times \Lambda_{T_h^i/2}\left[\tau - (m+n+1)\frac{T_h^i}{2} + T_c\right] \\
&= \frac{1}{4} \sum_{m=0}^{2N_i-1} \sum_{n=0}^{2N_i-1} (-1)^{\lfloor \frac{m+1}{2} \rfloor + \lfloor \frac{n+1}{2} \rfloor} T_h^i \\
&\quad \times \Lambda_{T_h^i/2}\left[\tau - (m+n+1-2N_i)\frac{T_h^i}{2}\right]
\end{aligned} \tag{38}$$

Finally, by substituting (34) and (38) into (28), the expression of the ACF for the nonconstant-envelope FH-AltBOC signal is derived as follows:

$$\begin{aligned}
R_{\mathrm{NCE}}(\tau) = \frac{1}{L_c T_c} \sum_{i=0}^{M-1} l_i T_h^i \Bigg\{ & 2 \sum_{m=0}^{N_i-1} \sum_{n=0}^{N_i-1} (-1)^{m+n+1} \\
& \times \Lambda_{T_h^i}\left[\tau - (m+n+1-N_i) T_h^i\right] \\
& + \sum_{m=0}^{2N_i-1} \sum_{n=0}^{2N_i-1} (-1)^{\lfloor \frac{m+1}{2} \rfloor + \lfloor \frac{n+1}{2} \rfloor} \\
& \times \Lambda_{T_h^i/2}\left[\tau - (m+n+1-2N_i)\frac{T_h^i}{2}\right] \Bigg\}
\end{aligned} \tag{39}$$

The derivation of the ACF for the constant-envelope FH-AltBOC signal is similar to that for the nonconstant-envelope FH-AltBOC signal. The ACF for the constant-envelope FH-AltBOC signal can be expressed as

$$\begin{aligned}
R_{\mathrm{CE}}(\tau) = \frac{1}{2L_c T_c} \sum_{i=0}^{M-1} \Big[& sc_d\left(t, f_h^i\right) sc_d\left(t+\tau, f_h^i\right) \\
& + sc_d\left(t - T_s/4, f_h^i\right) sc_d\left(t - T_s/4 + \tau, f_h^i\right) \\
& + sc_p\left(t, f_h^i\right) sc_p\left(t+\tau, f_h^i\right) \\
& + sc_p\left(t - T_s/4, f_h^i\right) sc_p\left(t - T_s/4 + \tau, f_h^i\right) \Big] \times l_i
\end{aligned} \tag{40}$$

Let $sc_{d1}\left(t, f_h^i\right) = sc_d\left(t, f_h^i\right)$, $sc_{d2}\left(t, f_h^i\right) = sc_d\left(t - T_s/4, f_h^i\right)$, $sc_{p1}\left(t, f_h^i\right) = sc_p\left(t, f_h^i\right)$, and $sc_{p2}\left(t, f_h^i\right) = sc_p\left(t - T_s/4, f_h^i\right)$.

Then, the ACF for the constant-envelope FH-AltBOC signal can be expressed as

$$\begin{aligned}
R_{\mathrm{CE}}(\tau) &= \frac{1}{2L_c T_c} \sum_{i=0}^{M-1} \left[\begin{array}{l} R_{sc_{d1}}^i(\tau) + R_{sc_{d2}}^i(\tau) + \\ R_{sc_{p1}}^i(\tau) + R_{sc_{p2}}^i(\tau) \end{array} \right] \times l_i \\
&= \frac{1}{2L_c T_c} \sum_{i=0}^{M-1} \left[\begin{array}{l} sc_{d1}\left(\tau, f_h^i\right) \otimes sc_{d1}\left(-\tau, f_h^i\right) \\ + sc_{d2}\left(\tau, f_h^i\right) \otimes sc_{d2}\left(-\tau, f_h^i\right) \\ + sc_{p1}\left(\tau, f_h^i\right) \otimes sc_{p1}\left(-\tau, f_h^i\right) \\ + sc_{p2}\left(\tau, f_h^i\right) \otimes sc_{p2}\left(-\tau, f_h^i\right) \end{array} \right] \times l_i
\end{aligned} \tag{41}$$

According to the definition, $sc_{d1}\left(\tau, f_h^i\right)$, $sc_{d2}\left(\tau, f_h^i\right)$, $sc_{p1}\left(\tau, f_h^i\right)$, and $sc_{p2}\left(\tau, f_h^i\right)$ have the following property:

$$\begin{cases}
sc_{d1}\left(\tau, f_h^i\right) = sc_{d1}\left(T_c - \tau, f_h^i\right) \\
sc_{d2}\left(\tau, f_h^i\right) = -sc_{d2}\left(T_c - \tau, f_h^i\right) \\
sc_{p1}\left(\tau, f_h^i\right) = sc_{p1}\left(T_c - \tau, f_h^i\right) \\
sc_{p2}\left(\tau, f_h^i\right) = -sc_{p2}\left(T_c - \tau, f_h^i\right)
\end{cases} \tag{42}$$

Furthermore, $sc_{d1}\left(\tau, f_h^i\right)$, $sc_{d2}\left(\tau, f_h^i\right)$, $sc_{p1}\left(\tau, f_h^i\right)$, and $sc_{p2}\left(\tau, f_h^i\right)$ can also be expressed as

$$\begin{aligned}
&sc_{d1}\left(t, f_h^i\right) \\
&= \mu_{T_h^i/4}(t) \otimes \sum_{m=0}^{4N_i-1} \left[\frac{\sqrt{2}}{4} (-1)^{\lfloor \frac{m+1}{4} \rfloor} \right. \\
&\quad \left. + \frac{1}{2}(-1)^{\lfloor \frac{m+2}{4} \rfloor} + \frac{\sqrt{2}}{4}(-1)^{\lfloor \frac{m+3}{4} \rfloor} \right] \delta\left(t - \frac{mT_h^i}{4}\right) \\
&sc_{d2}\left(t, f_h^i\right) \\
&= \mu_{T_h^i/4}(t) \otimes \sum_{m=0}^{4N_i-1} \left[\frac{\sqrt{2}}{4} (-1)^{1+\lfloor \frac{m+3}{4} \rfloor} \right. \\
&\quad \left. + \frac{1}{2}(-1)^{\lfloor \frac{m}{4} \rfloor} + \frac{\sqrt{2}}{4}(-1)^{\lfloor \frac{m+1}{4} \rfloor} \right] \delta\left(t - \frac{mT_h^i}{4}\right) \\
&sc_{p1}\left(t, f_h^i\right) \\
&= \mu_{T_h^i/4}(t) \otimes \sum_{m=0}^{4N_i-1} \left[\frac{\sqrt{2}}{4} (-1)^{1+\lfloor \frac{m+1}{4} \rfloor} \right. \\
&\quad \left. + \frac{1}{2}(-1)^{\lfloor \frac{m+2}{4} \rfloor} + \frac{\sqrt{2}}{4}(-1)^{1+\lfloor \frac{m+3}{4} \rfloor} \right] \delta\left(t - \frac{mT_h^i}{4}\right) \\
&sc_{p2}\left(t, f_h^i\right) \\
&= \mu_{T_h^i/4}(t) \otimes \sum_{m=0}^{4N_i-1} \left[\frac{\sqrt{2}}{4} (-1)^{\lfloor \frac{m+3}{4} \rfloor} \right. \\
&\quad \left. + \frac{1}{2}(-1)^{\lfloor \frac{m}{4} \rfloor} + \frac{\sqrt{2}}{4}(-1)^{1+\lfloor \frac{m+1}{4} \rfloor} \right] \delta\left(t - \frac{mT_h^i}{4}\right)
\end{aligned} \tag{43}$$

By substituting (42) and (43) into (41), the expression of the ACF for the constant-envelope FH-AltBOC signal can be

derived:

$$R_{\mathrm{CE}}(\tau) = \frac{1}{L_c T_c} \sum_{i=0}^{M-1} \sum_{m=0}^{4N_i-1} \sum_{n=0}^{4N_i-1} l_i T_h^i \left[\frac{1}{16}(-1)^{\lfloor \frac{m}{4} \rfloor + \lfloor \frac{n}{4} \rfloor + 1} + \frac{1}{16}(-1)^{\lfloor \frac{m+2}{4} \rfloor + \lfloor \frac{n+2}{4} \rfloor} + \frac{1}{8}(-1)^{\lfloor \frac{m+1}{4} \rfloor + \lfloor \frac{n+3}{4} \rfloor} \right] \times \Lambda_{T_h^i/4} \left[\tau - (m+n+1-4N_i)\frac{T_h^i}{4} \right] \quad (44)$$

The above derivation yields expressions of the ACFs for nonconstant and constant-envelope FH-AltBOC modulations.

REFERENCES

[1] N. Zhu, J. Marais, D. Betaille, and M. Berbineau, "GNSS position integrity in urban environments: A review of literature," *IEEE Trans. Intell. Transp. Syst.*, vol. 19, no. 9, pp. 2762–2778, Sep. 2018.

[2] X. Gan, C. Sheng, H. Zhang, and L. Huang, "Combination of asynchronous array pseudolites and GNSS for outdoor localization," *IEEE Access*, vol. 7, pp. 38550–38557, 2019.

[3] Z. Yao and M. Lu, "Signal multiplexing techniques for GNSS: The principle, progress, and challenges within a uniform framework," *IEEE Signal Process. Mag.*, vol. 34, no. 5, pp. 16–26, Sep. 2017.

[4] L. Lestarquit, G. Artaud, and J. L. Issler, "AltBOC for dummies or everything you always wanted to know about AltBOC," in *Proc. ION GNSS*, Savannah, GA, USA, Sep. 2008, pp. 961–970.

[5] N. C. Shivaramaiah, A. G. Dempster, and C. Rizos, "Time-multiplexed offset-carrier QPSK for GNSS," *IEEE Trans. Aerosp. Electron. Syst.*, vol. 49, no. 2, pp. 1119–1138, Apr. 2013.

[6] Z. Tang, H. Zhou, J. Wei, T. Yan, Y. Liu, Y. Ran, and Y. Zhou, "TD-AltBOC: A new COMPASS B2 modulation," *Sci. China Phys., Mech. Astron.*, vol. 54, no. 6, pp. 1014–1021, Jun. 2011.

[7] K. Zhang, H. Zhou, and F. Wang, "Unbalanced AltBOC: A compass B1 candidate with generalized MPOCET technique," *GPS Solutions*, vol. 17, no. 2, pp. 153–164, Apr. 2013.

[8] K. Zhang, "Generalised constant-envelope DualQPSK and AltBOC modulations for modern GNSS signals," *Electron. Lett.*, vol. 49, no. 21, pp. 1335–1337, Oct. 2013.

[9] Z. Yao, J. Zhang, and M. Lu, "ACE-BOC: Dual-frequency constant envelope multiplexing for satellite navigation," *IEEE Trans. Aerosp. Electron. Syst.*, vol. 52, no. 1, pp. 466–485, Feb. 2016.

[10] X. Huang, X. Zhu, X. Tang, H. Gong, and G. Ou, "GCE-BOC modulation: A generalized multiplexing technology for modern GNSS dual-frequency signals," in *Proc. CSNC*, vol. 2, 2015, pp. 47–55.

[11] T. Yan, J. Wei, Z. Tang, Z. Zhou, and X. Xia, "General AltBOC modulation with adjustable power allocation ratio for GNSS," *J. Navigat.*, vol. 69, no. 3, pp. 531–560, May 2016.

[12] X. Huang, X. Zhu, G. Ou, and X. Tang, "Asymmetric AltBOC modulation and its generalised form for BeiDou B2 signals," *Electron. Lett.*, vol. 52, no. 2, pp. 146–148, Jan. 2016.

[13] J. Zhang, Z. Yao, and M. Lu, "Applications and low-complex implementations of ACE-BOC multiplexing," in *Proc. ION ITM*, San Diego, CA, USA, Jan. 2014, pp. 781–791.

[14] F. Guo, Z. Yao, and M. Lu, "BS-ACEBOC: A generalized low-complexity dual-frequency constant-envelope multiplexing modulation for GNSS," *GPS Solutions*, vol. 21, no. 2, pp. 561–575, Apr. 2017.

[15] Y. Zhou and Y. Pan, "Unambiguous tracking method for alternative binary offset carrier modulated signals based on pseudo correlation function technique," *IEEE Commun. Lett.*, vol. 19, no. 3, pp. 371–374, Mar. 2015.

[16] M. K. Simon, J. K. Omura, R. A. Scholtz, and B. K. Levitt, *Spread Spectrum Communications Handbook*, 2nd ed. New York, NY, USA: McGraw-Hill, 1994, pp. 1158–1163.

[17] R. L. Peterson, R. E. Ziemer, and D. E. Borth, *Introduction to Spread Spectrum Communications*. Upper Saddle River, NJ, USA: Prentice-Hall, 1995, pp. 47–83.

[18] D. Torrieri, "Frequency-hopping systems," in *Principles of Spread-Spectrum Communication Systems*, 3rd ed. Heidelberg, Germany: Springer, 2015, pp. 147–200.

[19] L. M. Wolff and S. Badri-Hoeher, "Convolutionally coded hopping pattern for MFSK modulation in underwater acoustic communication," *IEEE Access*, vol. 7, pp. 95569–95575, 2019.

[20] L. W. Couch, *Digital & Analog Communication Systems*, 8th ed Upper Saddle River, NJ, USA: Prentice-Hall, 2001, pp. 426–428.

[21] J. W. Betz, "Binary offset carrier modulations for radionavigation," *Navigation*, vol. 48, no. 4, pp. 227–246, Dec. 2001.

[22] J. W. Betz, "The offset carrier modulation for GPS modernization," in *Proc. ION ITM*, San Diego, CA, USA, Jan. 1999, pp. 639–648.

[23] C. Ma, G. Lachapelle, and M. E. Cannon, "Implementation of a software GPS receiver," in *Proc. ION GNSS*, Long Beach, CA, USA, Sep. 2004, pp. 956–970.

[24] J. W. Betz and K. R. Kolodziejski, "Generalized theory of code tracking with an early-late discriminator part I: Lower bound and coherent processing," *IEEE Trans. Aerosp. Electron. Syst.*, vol. 45, no. 4, pp. 1538–1556, Oct. 2009.

[25] J. W. Betz and K. R. Kolodziejski, "Generalized theory of code tracking with an early-late discriminator part II: Noncoherent processing and numerical results," *IEEE Trans. Aerosp. Electron. Syst.*, vol. 45, no. 4, pp. 1557–1564, Oct. 2009.

[26] R. Pickholtz, D. Schilling, and L. Milstein, "Theory of spread-spectrum Communications–A tutorial," *IEEE Trans. Commun.*, vol. COM-30, no. 5, pp. 855–884, May 1982.

[27] J. Wu, X. Tang, Z. Li, C. Li, and F. Wang, "Cascaded interference and multipath suppression method using array antenna for GNSS receiver," *IEEE Access*, vol. 7, pp. 69274–69282, 2019.

[28] G. W. Hein, J.-A. Avila-Rodriguez, S. Wallner, A. R. Pratt, J. Owen, J. Issler, J. W. Betz, C. J. Hegarty, S. Lenahan, J. J. Rushanan, A. L. Kraay, and T. A. Stansell, "MBOC: The new optimized spreading modulation recommended for GALILEO l1 OS and GPS L1C," in *Proc. IEEE/ION Position, Location, Navigat. Symp.*, San Diego, CA, USA, Apr. 2006, pp. 883–892.

JIANGANG MA received the B.S. degree from Xidian University, Xi'an, China. He is currently pursuing the Ph.D. degree with the School of Electronics and Information Engineering, Xi'an Jiaotong University, Xi'an. His current research interests focus on GNSS signal design and signal processing.

YIKANG YANG received the B.S., M.S., and Ph.D. degrees in electronics engineering from Xi'an Jiaotong University, Xi'an, China. He is currently a Professor with the School of Electronics and Information Engineering, Xi'an Jiaotong University. His research interests include satellite navigation, inter-satellite link, spacecraft telemetry, tracking, and command (TT&C), and signal processing.